Current–voltage characteristics of nonplanar cold field emitters

Christopher John Edgcombe[a)]
Department of Physics, University of Cambridge, Cambridge CB3 0HE and Granta Electronics Ltd., 25 St. Peter's Road, Coton Cambridge CB3 7PR, United Kingdom

Adam Michael Johansen
Department of Engineering, University of Cambridge, Cambridge CB2 1PZ, United Kingdom

(Received 6 January 2003; accepted 19 May 2003; published 31 July 2003)

Conventional Fowler–Nordheim theory assumes that the emitter is planar, while most tips used in practice have curved emitting surfaces. Using a revised potential distribution, standard image theory and a dimensionless parameter x, we express the experimental current as a multiple σ of the current calculated using standard free-electron supply. A plot of $\sigma(x)$ for one carbon emitter shows a maximum at a value of x corresponding to the known emitter radius. The calculated field strength at the emitter surface varies little with x. The values found for σ are sensitive to the accuracy of calculation and, to test the theory further, it is desirable both to improve the modelling of image effects and to obtain measurements of current–voltage characteristics and emitting radii together for more types of emitter. © *2003 American Vacuum Society.* [DOI: 10.1116/1.1591748]

I. INTRODUCTION

Conventional Fowler–Nordheim (FN) theory for a planar surface does not represent accurately the experimental behavior of single cold field emitters. For example, when an amorphous carbon tip was considered,[1] the work function deduced from the FN plot by planar theory was 66% of the value measured by Kelvin probe microscopy. Also the emitter radius deduced from the intercept of the same plot was about 260% of the value measured by scanning electron microscopy.

We therefore looked for modifications of the established theory to give a better description of real emitters. There are many ways in which the simple theory might be improved to provide a more accurate model of their behavior. One obvious weakness of the known theory is that it applies to planar surfaces, while most field emitting surfaces used in practice are curved, typically with a radius of curvature between 1 nm and 1 μm. Here we consider the emission calculated from a potential distribution typical of a spherical surface supported on a tapered shank. We require a model for the potential which is accurate in the barrier region, that is within a distance of the order of 1 nm from the emitter surface.

II. POTENTIAL IN THE BARRIER REGION

A. Analytical models of potential

A solution to Laplace's equation for the potential ϕ in a rotationally symmetric system can be obtained in spherical coordinates as

$$\phi=\left(A_\nu\left(\frac{r}{a}\right)^\nu+B_\nu\left(\frac{r}{a}\right)^{-\nu-1}\right)P_\nu(\cos\theta), \tag{1}$$

where P_ν represents a Legendre polynomial of degree ν, and a, A_ν, and B_ν are constants. The general solution consists of a sum or integral of products of functions of r and θ, of the form shown in Eq. (1), over all values of ν. The constants are determined by the boundary conditions. If the emitter surface consisted of a perfect cone of semiangle α, with the origin of coordinates taken as the apex of this cone, then it would be possible to use only those values of ν for which

$$P_\nu(\cos(\pi-\alpha))=0. \tag{2}$$

This condition makes the potential zero at all values of r on the conical surface. Hence if such a surface is defined to coincide with the shank of a real emitter, it cannot give a good model of the potential on the axis near the real emitting surface.

Ideally, we wish to ensure that the potential is constant over a shape fitting the surface of an emitter, by choice of all A_ν and B_ν. A way of achieving this was described by Dyke and Dolan,[2] who considered the union of two conducting volumes: a cone of semiangle α and a sphere of radius a centered at the apex of the cone. A potential that is constant over the surface of this structure is, subject to condition (2),

$$\phi=A_\nu\left(\left(\frac{r}{a}\right)^\nu-\left(\frac{r}{a}\right)^{-\nu-1}\right)P_\nu(\cos\theta). \tag{3}$$

The form of the zero equipotential of this "core structure" ($r=a$ or $\theta=\alpha$) is unlikely to be used for an emitter in practice, but some of the other equipotentials generated outside this structure do resemble typical shapes of practical emitters. Hence, in principle, the potential given by Eq. (3) is usable to model emission. The values of a and ν needed for this model differ from those for the hemispherical cap and shank of the real emitter, and the relation between them has to be found for each shape of emitter; also since the value of ν is likely to be between 0 and 0.5, P_ν is only available as an infinite sum, not a polynomial. Thus in practice appreciable computation is needed to use relation (3) directly. In view of this, we decided to seek simpler functions of r and θ that would provide acceptable approximations to ϕ within the barrier region.

[a)]Electronic mail: cje1@cam.ac.uk

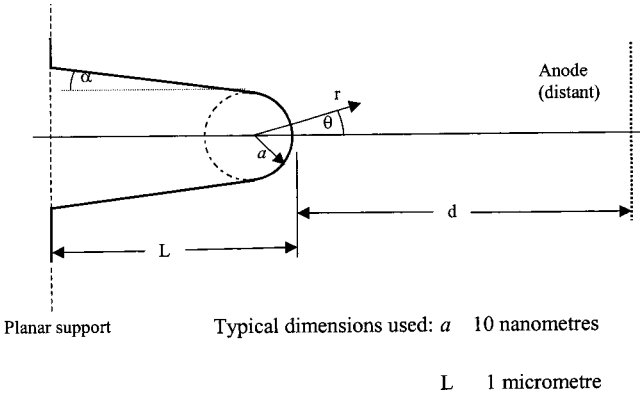

FIG. 1. Geometry and notation for tip.

B. Approximation for potential near the emitter

As in earlier computations[1] of field enhancement factor, we modeled the emitter as a spherical cap of physical radius a, supported on a conical shank of total length L and semi-angle α, as shown in Fig. 1. From the computed distribution of potential ϕ, we calculated $F=\partial\phi/\partial r$, the negative of the radial electric field, on the axis ($\theta=0$), as a function of distance r from the center of curvature of the emitter, as shown in Fig. 2. This plot shows that the radial field on the axis of a curved emitter is not constant, as is assumed when planar theory is applied. Instead it falls off approximately as $(a/r)^2$, where a is the radius of curvature of the emitting surface.

We also examined the dependence of F at the emitter surface on angle θ to the axis, as shown in Fig. 3. It can be seen that, over the range $\theta<70°$, F/F_0 can be fitted approximately by $\cos\theta/2$. This result agrees with a calculation of Dyke and Dolan,[2] as shown in their Fig. 7 for their emitter shape B, which is very similar to our sphere-on-cone model. Thus we have, over the limited ranges of r and θ that are of interest for calculating emission

on $\theta=0$,

$$\partial\phi/\partial r\approx F_0(a/r)^2$$

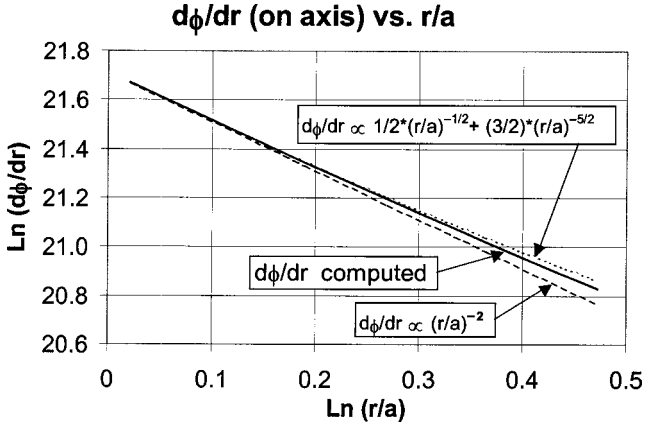

FIG. 2. Calculated variation of radial field on the axis of a curved emitter, with distance from the center of curvature.

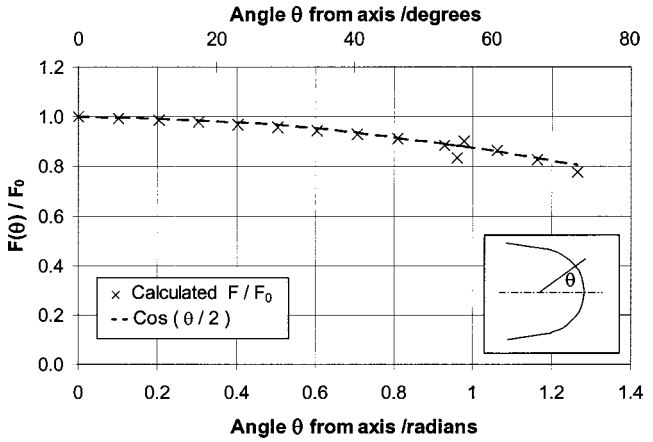

FIG. 3. Calculated variation of field strength at the surface of a curved emitter, with angle from the axis.

on $r=a$,

$$\partial\phi/\partial r\approx F_0\cos(\theta/2),$$

where F_0 is the value of F at $r=a$ on the axis.

When the general solution for ϕ is expressed in the form

$$\phi=\sum_\nu R_\nu(r)\Theta_\nu(\theta),$$

then the corresponding expression for F is

$$F=\sum_\nu (\partial R_\nu/\partial r)\Theta_\nu(\theta).$$

In general, R_ν and $\partial R_\nu/\partial r$ are different functions of ν, and so ϕ and F can be expected to vary differently with θ. However, if ϕ is represented, accurately or approximately, by a single product of functions of r and θ, then ϕ and $\partial\phi/\partial r$ are given by

$$\phi=R(r)\Theta(\theta),\quad \partial\phi/\partial r=(\partial R/\partial r)\Theta(\theta).$$

Hence when ϕ can be represented by a single product of functions of r and of θ, then ϕ and $\partial\phi/\partial r$ have the same dependence on θ.

From the dependence of $\partial\phi/\partial r$ on θ at $r=a$ as found above, $\Theta(\theta)=\cos\theta/2$. Also from the dependence of $\partial\phi/\partial r$ on r at $\theta=0$, $\partial R/\partial r=F_0(a/r)^2$. Hence we can obtain $R(r)$ by integrating $F_0(a/r)^2$ with respect to r, subject to the condition that R is to be zero on $r=a$. The resulting expression for ϕ is

$$\phi(r,\theta)=aF_0\left(1-\frac{a}{r}\right)\cos\theta/2, \tag{4}$$

where F_0 is the magnitude of field strength at the emitter surface, on the axis. Since $F=F_0\cos\theta/2$, Eq. (4) can also be written as

$$\phi(r,\theta)=aF\left(1-\frac{a}{r}\right)$$

and this form will be used where it is not necessary to show the dependence on θ explicitly.

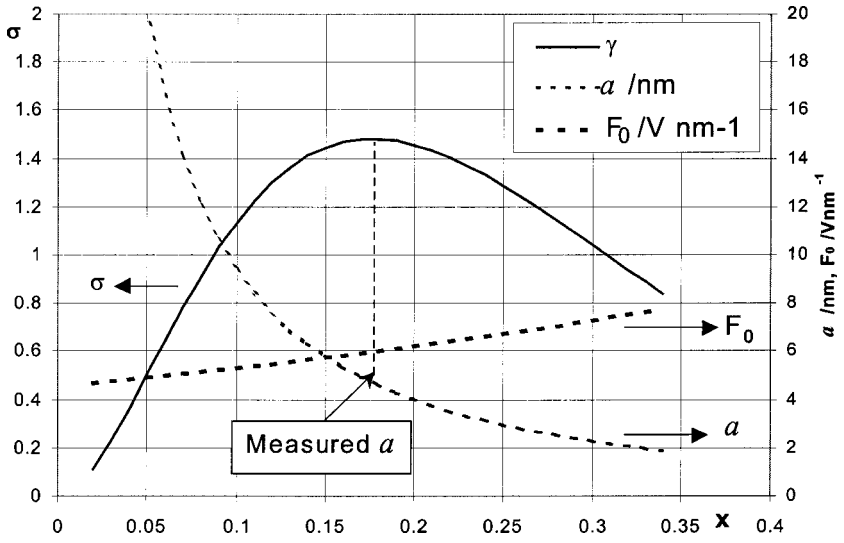

FIG. 4. Parameters a, F_0, and σ calculated as functions of x, with consistent q found by iteration.

C. Image potential

The image potential was approximated by that of an electron of charge $-e$ near a sphere of radius a (coinciding with the spherical part of the emitter surface). Additional charge was included at the center of the sphere to keep the total induced charge equal to that of the electron. The image charges used were thus $+ea/r$ at radius a^2/r, and $+e(1-a/r)$ at the center of curvature, giving an image potential

$$\phi_m=\frac{e}{8\pi\varepsilon_0 a}\left[\left(\frac{r^2}{a^2}-1\right)^{-1}+\frac{2a}{r}-\frac{a^2}{r^2}\right].$$

D. Total potential

The total potential energy V used was thus

$$V(r,\theta)=W-aeF\left(1-\frac{a}{r}\right)-Waq\left(\frac{a}{r^2-a^2}+\frac{2}{r}-\frac{a}{r^2}\right)$$

$$=W\left[1-\frac{\cos(\theta/2)}{x}\left(1-\frac{1}{\rho}\right)-q\left(\frac{1}{\rho^2-1}+\frac{2}{\rho}-\frac{1}{\rho^2}\right)\right],$$

where W is the work function of the surface,

$$x=\frac{W}{aeF_0},\quad \rho=\frac{r}{a},$$

and

$$q=\frac{e^2}{8\pi\varepsilon_0 aW}.$$

III. TOTAL EMITTED CURRENT

With these approximations, and after integrating over θ, the total emitted current can be written as[3,4]

$$I=\frac{\sigma\Omega a^2 c_1 F_0^2}{W\ w^2(f)}\exp\left[\frac{-c_2 W^{3/2} f(x,q)}{F_0 x}\right]. \quad (5)$$

Here σ is the ratio of experimental current to that calculated from the free-electron supply function, Ω is the effective solid angle of emission (which accounts for the variation of current density with angle), and c_1 and c_2 are standard constants. The functions $f(x,q)$ and $w(f)$ are defined by

$$f(x,q)=\frac{3}{2}\int_{\rho_1}^{\rho_2}\left[1-\frac{1}{x}\left(1-\frac{1}{\rho}\right)-q\left(\frac{1}{\rho^2-1}+\frac{2}{\rho}-\frac{1}{\rho^2}\right)\right]^{1/2}d\rho,$$

$$w(f)=\left[f(x,q)+2x\frac{\partial f}{\partial x}-2q\frac{\partial f}{\partial q}\right]\Big/ 3x.$$

The limits ρ_1 and ρ_2 are values of ρ, greater than unity, at which the integrand is zero.

The ratio f/x is used in place of the function $\nu(y)$ used in earlier theory; likewise, $w(x,q)$ replaces $t(y)$. The product $(F_0 x)$ does not depend on F_0, so the exponent in Eq. (5) can also be written as $[-c_2 aeW^{1/2} f(x,q)]$.

The factor σ has been included explicitly in Eq. (5) to show the relation between experimental current and that deduced using the free-electron supply function. Its value for a particular experiment can be estimated if W, a, and F_0 are known. However, often the values of one or more of these

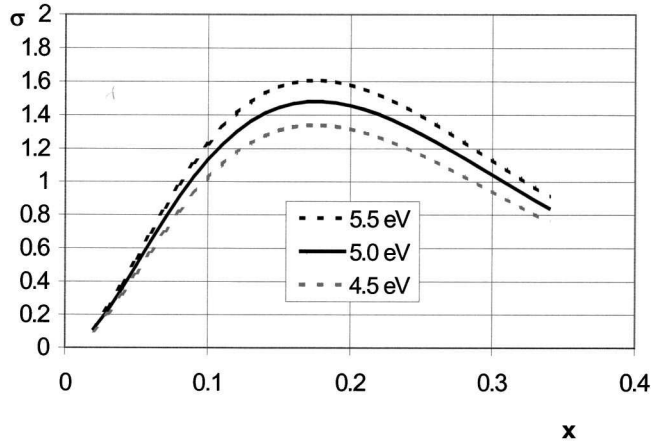

FIG. 5. σ as a function of x for three values of work function W.

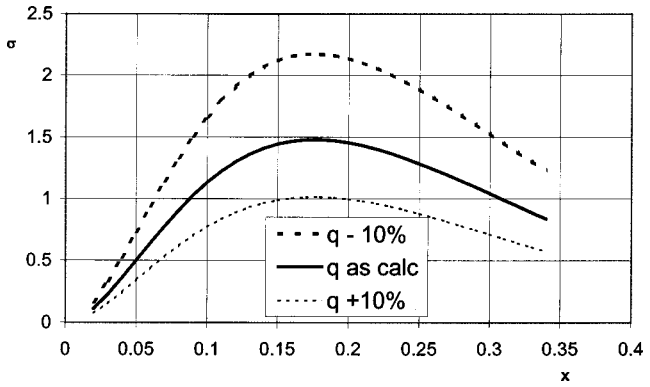

FIG. 6. σ as a function of x for three multiples of q found by iteration.

parameters is not known, and the question arises: within what range(s) can values of σ and the other parameters be determined from the experimental results ?

IV. PROBLEM OF EXTRACTION OF PARAMETERS FROM *I–V* RESULTS (WHEN *W*, *a* OR F_0 IS UNKNOWN)

The theory given above includes the radius of curvature of the emitter, and so has one parameter more than the planar theory. If more than two parameters are unknown they cannot be evaluated directly from the slope and intercept of the conventional FN plot using the relations above. However, we can use a pair of experimental values of the FN slope and intercept, together with the mid-range anode voltage and the known or assumed work function, to find σ, a, and F_0 as functions of the dimensionless parameter x (with iteration for the value of q). Then if any one of σ, a, or F_0 is known, the others can also be found.

We have investigated this calculation using data for two emitters for which some information was known about the radii of curvature. These emitters were: (a) an amorphous carbon tip made by Antognozzi *et al.*[5] using e-beam deposition and (b) a carbon nanotube with current–voltage ($I-V$) characteristic as shown in Fig. 6.3 of the thesis by Fransen.[6] We also calculated results for (c) a pointed tungsten emitter with $I-V$ characteristics shown as Fig. 6.7 of the thesis by James.[7]

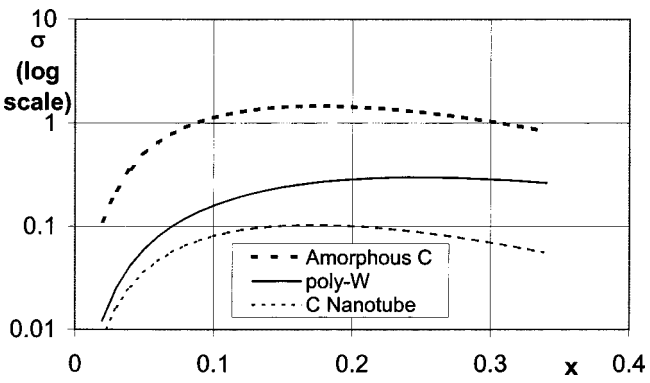

FIG. 7. σ as a function of x for three emitters.

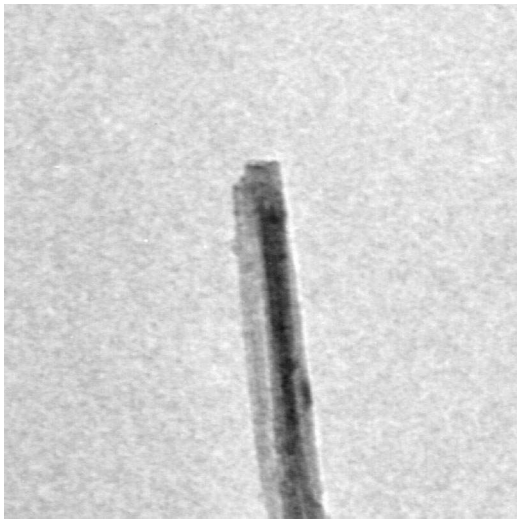

FIG. 8. Detail of tip of nanotube studied by Fransen (from Ref. 6).

In addition to calculating σ, a, and F_0 as functions of x, we have investigated the sensitivity of these calculations to variations in W and q.

The functions f and w were evaluated numerically for given values of x, with iteration for q. It was found necessary to evaluate f with great accuracy, both to keep the calculation of w accurate and to ensure consistent convergence.

A. Amorphous carbon tip–σ, field strength, and radius of curvature

Results for σ, a, and F_0 as functions of x for an amorphous carbon tip are shown in Fig. 4. The calculated emitter radius a falls rapidly as x increases, but the field strength F_0 remains within a much smaller range.

The maximum σ for the amorphous carbon tip occurs at $x=0.18$, for which the calculated tip radius is 4.8 nm. This agrees well with the measured value of 5.0 ± 1.5 nm. The good agreement suggests that the maximum of σ might conveniently be used to indicate the value of x corresponding to the experimental value of a. However, in this case the calculated value of σ at its maximum exceeds 1, implying that the current available exceeds that from the free-electron model. It seems possible that the free-electron density may be exceeded if there is an appreciable density of surface states. It is clearly desirable to compare radii calculated in this way with measured values, for other emitters of known dimensions.

1. Variation of σ with W

Figure 5 shows the effect on σ of varying W, using data for the amorphous carbon tip. The value of x at which σ is maximum varies by less than 0.005 for the change of ±0.5 eV in work function.

2. Variation of σ with q

The effect on σ of varying the image parameter q, using data for the amorphous carbon tip, is shown in Fig. 6. The value of x at which σ is maximum varies by less than 0.005

for the change of $\pm 10\%$ in q. However, the value of σ at the maximum varies by a factor of about 1.5. The calculation of σ is thus sensitive to the accuracy of estimation of the image potential.

V. COMPARISON OF EMITTERS

Figure 7 shows σ for three emitters (using a log scale for σ) as functions of x. By considering the form of σ from Eq. (5), it can be seen that the shape of the curve plotted is that of a function like $x^2 \exp[(\text{constant})\ af(x,q)]$; as x increases, a decreases so the curve passes through a maximum. The smaller the radius of the experimental emitter is, the greater will be the value of x at which the maximum occurs.

The two forms of carbon yield graphs of very similar shapes. This suggests that the emitters tested have similar radii of curvature. The maximum values of σ differ by a factor of about 14. This appears to indicate that the mid-range current drawn from the nanotube was smaller than that from the amorphous tip, at their respective anode voltages, by the same factor.

For the nanotube, the value of a corresponding to the maximum of σ is 5.4 nm, which is appreciably less than half the measured diameter of 44 nm. That this small value for a is possible can be seen from a micrograph of the end of the same nanotube (Fig. 8). The micrograph shows that the tip profile is not a smooth hemisphere, but is irregular and so may indeed emit principally from a radius smaller than half the diameter.

VI. CONCLUSIONS

Conventional Fowler–Nordheim (FN) theory for a planar surface does not represent accurately the experimental behavior of single cold field emitters with curved emitting surfaces.

Using (1) an analytic approximation to the computed potential near the emitter, (2) the image potential for a spherical surface, and (3) the free-electron density of states, and taking into account (4) the variation of current density over the emitter, we have written the total current as a function of parameters x and q and the ratio σ of the experimental and theoretical values of current.

From experimental measurements of the current–voltage relation, σ, the field strength F and the emitter radius a can be calculated as functions of x, with q determined by iteration. We find that F increases slowly, and a falls rapidly, as x increases. In one case the ratio σ has a maximum at the value of x corresponding to the experimental emitter radius, but it is not yet clear whether this result occurs more generally.

For these calculations, the image potential has been obtained from the image in a sphere whose surface coincides with the emitting surface of the tip. This obviously does not account for the presence of the shank of the tip. Inaccuracy of the image potential of the order of 10% is thus a possible reason why the experimental value of supply function (or density of states) appears to exceed the free-electron value, in this amorphous carbon emitter. A better model for the image potential is desirable.

To determine further how useful the technique outlined here may be for extracting information from FN plots, it is desirable to obtain measurements of both the $I-V$ characteristic and emitter radius together, for individual tips, of both metallic and other types of emitter.

ACKNOWLEDGMENTS

This continuing study was stimulated by the experimental work of Professor U. Valdrè and has benefited from discussion with him, Dr. R. G. Forbes, and Professor L. M. Brown.

APPENDIX: APPROXIMATIONS FOR FUNCTIONS *f*, *w* AND Ω

In an earlier article,[4] certain approximations were given for functions f and w. More accurate approximations for small x are now available, as follows:

$$f(x,0) \approx x + 4x^2/5,$$

$$w(x,q) \approx 1 + 4x/3 + 2q/3x.$$

In a still earlier article,[3] an approximate expression for the effective angle was given. In that article, following Eq. (22), the relation containing β should have read

$$F_0 = \beta V_a.$$

When the effective angle is evaluated using the approximation for $w(x,q)$ given above, the approximation becomes (ignoring terms of order q^2)

$$\Omega \approx 8\pi\left(1+\frac{4x_0}{3}\right)^2\left[-\frac{4q/3x_0}{6-S/V_a}+\frac{1}{5-S/V_a}-\frac{8x_0/3}{4-S/V_a}+\frac{16x_0^2/9}{3-S/V_a}\cdots\right].$$

In the same article,[3] the graphs plotted in Fig. 3 show $2g(x,q)$ and approximations to it, not $g\ (x,q)$ as stated.

[1] C. J. Edgcombe and U. Valdrè, Philos. Mag. B **82**, 987 (2002).
[2] W. P. Dyke and W. W. Dolan, Adv. Electron. Electron Phys. **8**, 89 (1956).
[3] C. J. Edgcombe, Philos. Mag. B **82**, 1009 (2002).
[4] C. J. Edgcombe, Ultramicroscopy **95**, 49 (2002).
[5] M. Antognozzi, A. Sentimenti, and U. Valdrè, Microsc. Microanal. Microstruct. **8**, 355 (1997).
[6] M. Fransen, *Towards High-Brightness, Monochromatic Electron Sources* (Technical University, Delft, The Netherlands, 1998). Reprinted from Appl. Surf. Sci. **146**, M. J. Fransen, Th. L. van Rooy, and P. Kruit, *Field emission energy distributions from individual multiwalled carbon nanotubes*, pp. 312–327, Copyright (1999), with permission from Elsevier.
[7] E. M. James, *Development and Characterisation of Advanced Field Emission Tips* (Department of Physics, University of Cambridge, Cambridge, UK, 1997).